

Effects of powder particle charging during RF plasma spheroidisation process

Milton Makhofane^{1*}, Hertzog Bissett¹ and Andrei Kolesnikov²

¹ The South African Nuclear Energy Corporation SOC Ltd (Necsa), Church Street West Ext, Pelindaba, Pretoria 0001, South Africa

² Department of Chemical, Metallurgical, and Material Engineering, Tshwane University of Technology, Pretoria 0185, South Africa

Abstract. Plasma spheroidisation converts irregular shaped particles to spherical morphology. The transformation occurs rapidly due to the high temperature of the plasma. This study highlights the effects of particle charging during spheroidisation of Ti6Al4V utilising a 15 kW radio frequency (RF) inductively coupled Tekna plasma system. Particles introduced into the RF plasma system acquire an equilibrium charge below 10^{-9} seconds. The determined Coulomb coupling parameters of the particle in the RF plasma indicates that the particle will form a Coulomb crystal when flowing through the plasma section.

1 Introduction

Plasma spheroidisation is a process of converting irregular shaped powder particle to a spherical morphology. The transformation is achieved by exposing irregular shaped powder particle to high temperature plasma gas *ca.* 10 000 K. The energy transferred from the plasma to the powder particles enables the powder particles to reach their melting point within milliseconds [1, 2]. A certain percentage of the powder particles will absorb enough energy to reach their boiling point and vaporise.

The plasma behaviour will be modified by the presence of the vapour of the processed material. The spheroidisation of Ti6Al4V alloy using radio frequency (RF) inductively coupled plasma generated from a mixture of argon and helium is considered as an example to explain the effect of powder particle charging during the spheroidisation process. The vapour of titanium, aluminium and vanadium have a lower first ionization energy compared with the plasma forming gasses, argon and helium, as seen in Table 1. The vapour will contribute a significant amount of electrons to the plasma, which will have an effect on the plasma properties, such as electrical conductivity and thermal conductivity that depend on the electron density in the plasma.

Table 1. Ionization energy of plasma gas and Ti6Al4V [3]

Material	Ionization energy, kJ/mol		
	1 st	2 nd	3 rd

* Corresponding author: milton.makhofane@necsa.co.za

Argon	1521	2666	3931
Helium	2372	5251	
Titanium	659	1310	2653
Aluminium	578	1817	27445
Vanadium	651	1414	2830

When irregular shaped Ti6Al4V powder particles are injected into the plasma, electrons and positive ions will move towards the powder particles. The powder particles will become negatively charged because the electrons have a higher thermal velocity than the positive ions under similar conditions due to the fact that electron has lower mass than positive ion. The positive ions reaching the powder particles will reduce the negative charge of the powder particles. The fluxes of electrons and positive ions reaching the powder particle will reach an equilibrium. However, the charge on the Ti6Al4V powder particles will remain negative even when the fluxes of electrons and ions is at equilibrium [4, 5]. This implies that a group of powder particles injected in a plasma will acquire a negative charge on their surfaces as the electrons reach the powder particles first, and as a result will repel each other. The repulsive force will keep the individual powder particles from agglomerating or clustering and also prevent inter-particle collisions. The positive ions in the plasma will be attracted by the negatively charged Ti6Al4V powder particles [5].

The argon and helium ions will heat the surface of the Ti6Al4V powder particle when they recombine with the electrons that are attached to the Ti6Al4V powder particle. Similarly, the Ti, Al and V ions will recombine with the electrons on the Ti6Al4V powder particle, contribute heat and condense on the Ti6Al4V powder particle. The condensation will result in surface growth of the Ti6Al4V powder particle which will ultimately increase the size of the powder particle. The aim of this paper is to establish the role that powder particle charging plays on the spheroidisation process.

2 Experimental

A 15 kW Tekna plasma system depicted in Figure 1 was used for the spheroidisation of Ti6Al4V powder. When the desired power of the RF plasma torch was reached, Ti6Al4V powder particles were introduced directly into the plasma by a water cooled feeding probe. The powder particles melt or vaporise depending on the amount of energy absorbed from the plasma. The powder particles are rapidly cooled by radiative loss and convection when exiting the plasma zone.

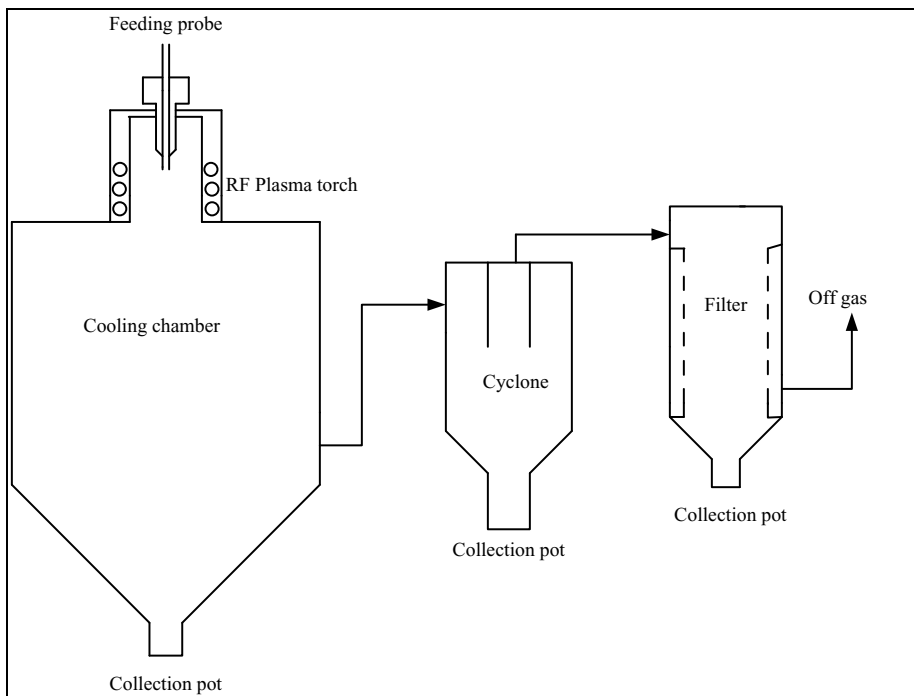


Fig. 1. Schematic of Tekna 15 kW plasma system

Powder particles were collected from the catch pot (collection pot) of the cooling chamber, cyclone and filter. Powder particles were also collected from the walls of the cooling chamber and the cyclone. The experimental conditions for spheroidising Ti6Al4V powder are given in Table 2.

Table 2. Operating parameters

Parameter	Value
Power, kW	11
System pressure, kPa _(absolute)	60
Plasma central gas (Ar), slpm	15
Plasma sheath gas (Ar + He), slpm	45
Powder carrier gas (Ar), slpm	2
Powder particle size, μm	63-90
Feeding rate, kg/h	0.67

The powder particle size distribution was measured using a Saturn DigiSizer II 5205 V1.03 and the morphologies were observed using a scanning electron microscope (SEM).

3 Results

The enthalpy of the plasma was determined from the ratio of the input power to the total gas flow rate, given in Table 2, and it was found to be *ca.* 10 722 kJ/kg. The temperature of the plasma was read from a table available in [6] using determined enthalpy and it was in the range of *ca.* 11 500 K [6]. The forward ionization reaction and reverse recombination

reaction of an atom in a plasma is illustrated using Equation 1. Assuming that the plasma was at local thermal equilibrium (LTE) where electron temperature is equal to the ion and neutral atom temperature, the composition of the plasma was estimated using the Gibbs minimisation method, Equation 2. The estimated plasma composition at 11 500 K is given in Table 3.



$$\Delta G = \Delta G^0 + RT \ln K \quad (2)$$

$$\text{Where: } K = \frac{[A^+][e^-]}{[A]}$$

Where: A is the neutral atom, A⁺ is the ionized atom (ion), e⁻ is the electron, ΔG is the Gibbs free energy (J/mol), ΔG⁰ is the Gibbs free energy at standard state (J/mol), R is the universal gas constant (8.3143 J/K.Mol), T is the temperature (K) and [] is the concentration (Mol/m³)

Table 3. Estimated composition of the plasma

Species	Density, particle/m ³	
Argon	Ar	1.94x10 ²³
	Ar ⁺	3.42x10 ¹⁹
	Ar ⁺⁺	1.51x10 ¹³
	Ar ⁺⁺⁺	8.91x10 ⁰³
Helium	He	1.82x10 ²³
	He ⁺	3.73x10 ¹⁷
	He ⁺⁺	2.22x10 ⁰⁵
Electrons	e	3.45x10 ¹⁹

The vaporized Ti6Al4V powder particle will absorb energy from the plasma and it will start to ionize. The spheroidised Ti6Al4V was processed to remove ultrafine powder particles of less than 4 μm. The powder with ultrafine particle accounted for 5.6wt.% of the total powder collected from the system after spheroidisation. The ultrafine powder particles are powder particles that were formed as a result of condensation of the vaporised Ti6Al4V. These are the powder particle that could not contribute to the surface growth of the bulk spheroidised powder particles. The electron density as a function of temperature is shown in Figure 2 for Ar/He plasma and Ar/He with evaporated Ti6Al4V. Equations 1 and 2 were used to determine the electron densities of the plasmas. It is evident that the evaporation of Ti6Al4V contributes a significant amount of electrons to the plasma. An increase in the plasma electrons will have an effect on the plasma direct current (dc) electrical conductivity. A plasma with evaporated Ti6Al4V has a high electrical conductivity (dc) compared with an Ar/He plasma, as shown in Figure 3. Equation 3 was used to determine the electrical conductivity (dc) of the weakly ionized Ar/He plasma [7, 8].

$$\sigma = \frac{n_e e^2 \tau_{en}}{m} \quad (3)$$

$$\text{Where: } \tau_{en} = \frac{4 \times 10^{15}}{n_n T_e^{1/2}}$$

Where: σ is the electrical conductivity (S/m), n_e is the electron density (particles/m³), e is the electron charge (1.6022 x 10⁻¹⁹ C), τ_{en} is the collision frequency, m is the mass of electron

(9.1094×10^{-31} kg), n_n is the neutral gas density(particles/m³), T_e is the plasma gas temperature (eV)

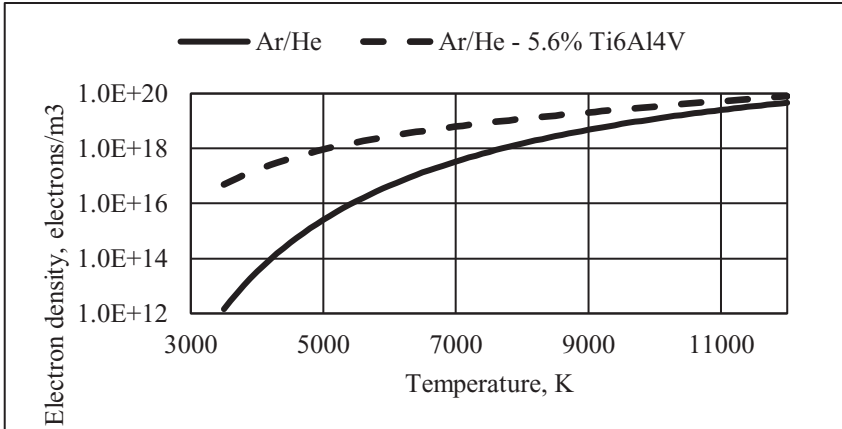


Fig. 2. Electron density of Ar/He plasma and Ar/He - 5.6% Ti6Al4V plasma

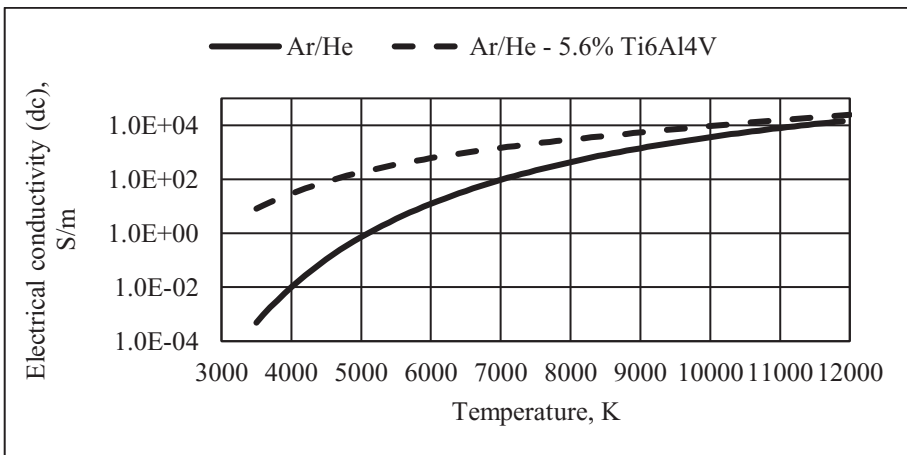


Fig. 3. Electrical conductivity of Ar/He plasma and Ar/He – 5.6% Ti6Al4V plasma

The powder particle size distribution of the raw Ti6Al4V and spheroidised Ti6Al4V are shown in Figure 4. The figure shows that the raw Ti6Al4V had a wider particle size distribution while the spheroidised Ti6Al4V had a narrower distribution. The plasma treated powder had *ca.* 5.6 wt% of particles below 4 μ m while the remainder had a size distribution of *ca.* 47 – 130 μ m. The powder particles below 4 μ m are formed by the vapour that condensed and solidified outside the plasma zone. The raw material had *ca.* 43vol.% of the particles below 47 μ m, *ca.* 53vol.% of the particles had size range of *ca.* 47 – 130 μ m and the remaining *ca.* 4vol% was particles above *ca.* 130 μ m. The raw material passed through the 90 μ m sieves and collected on top of the 63 μ m sieves. It was expected that the powder particles collected from on top of the 63 μ m will be within the 63 – 90 μ m range. The raw material had a wider distribution due to the aspect ratio of the irregular shaped powder particles.

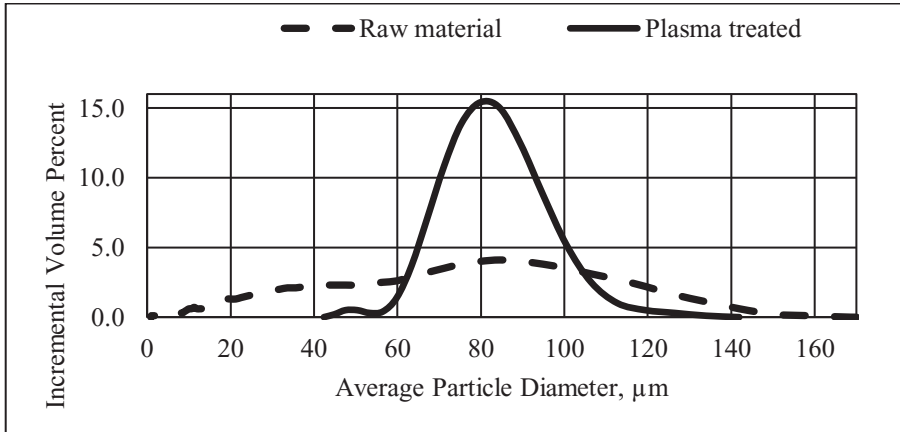


Fig. 4. Particle size distribution of the raw material and spheroidised material.

The amount of energy absorbed by the powder particles from the plasma depends on the powder particle size, position of the powder particles within the plasma and duration of powder particle in the plasma. The operating parameters (Table 2) for this experiment was optimum to spheroidise powder particles with size distribution from 63 – 90 µm, but high enough to vaporize powder particle below 63 µm. The absence of powder particle below 47 µm, except the ultrafine, from the plasma treated powder suggests that those particles merged to form particles with size greater than 47 µm. Particle growth due to direct collision of two particle in the plasma zone is highly unlikely due to the charge of the particle. The particle in the plasma will be negatively charge, as a result they will tend to repel each other. The only plausible explanation is that of recombination of the Ti⁺, Al⁺ and V⁺ ions with excess electrons of the negatively charge Ti6Al4V particle[5].

An analysis of the residence and melting time of powder particles in an RF plasma reported by [2] showed that the particle spent *ca.* 85% of the time in a molten state. This suggests that the Ti⁺, Al⁺ and V⁺ ions are likely to bond with the negatively charged molten Ti6Al4V particle resulting in growth of the particle [5].

Particle charging mechanism is used in electrostatic precipitator technology to remove micron size dust particles from a gas stream [9, 10]. Field charging and diffusion charging are the two charging mechanism used [9, 10]. Field charging does not play a significant role in the spheroidisation of Ti6Al4V using RF plasma due to the fact that the RF is electrodeless and also the field created by the displacement current occurs within the skin depth of the plasma which in most cases is located far from the particle injection location.

The injection point is located where the particle will come in contact with the thermal electrons and ions. A diffusion charging equation, derived by White [11], used to determine particle charging during an electrostatic precipitation process [11] can be applied to charging of powder particle in RF plasma. The significant factors that influence particle charging are; the particle diameter, density of electrons and ions, and the exposure time [12]. The charge on a particle as a function of time is determined by Equation 4, while the characteristic charging time is determined by Equation 5 [9, 11].

$$Q_d(t) = \frac{2\pi\epsilon_0 k T D_p}{e} \ln \left(1 + \frac{t}{\tau_d} \right) \quad (4)$$

$$\tau_d = \frac{\epsilon_0 \sqrt{8\pi k m T}}{e^2 n_{e,i} D_p} \quad (5)$$

Where: $Q_d(t)$ is the charge on a particle (C), ϵ_0 is permittivity of free space (8.845×10^{-12} F/m), k is the Boltzmann's constant (1.3806×10^{-23} J/K), T is the plasma temperature (K), t is the time (s), τ_d is the characteristic charging time (s).

The characteristic charging time of the particle introduced in the plasmas are shown in Figures 5 and 6 for a size ranging from 13-68 and 70-150 μm , respectively. Particle charging occurs at a faster time ($\sim 10^{-12}$ s) compared to the residence time ($\sim 10^{-3}$ s) [1, 2] of the powder particle in the plasma zone. The figures shows that the characteristic charging time is inversely proportional to the particle diameter. Therefore, the amount of charged species acquired by powder particle is a function of the particle diameter. Larger particle will have a high charge compared to small particles under similar conditions.

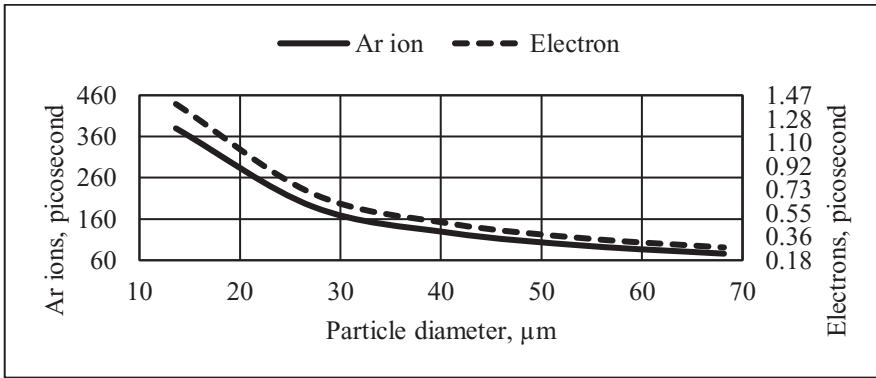


Fig. 5. Characteristic charging time of particles 13-68 μm

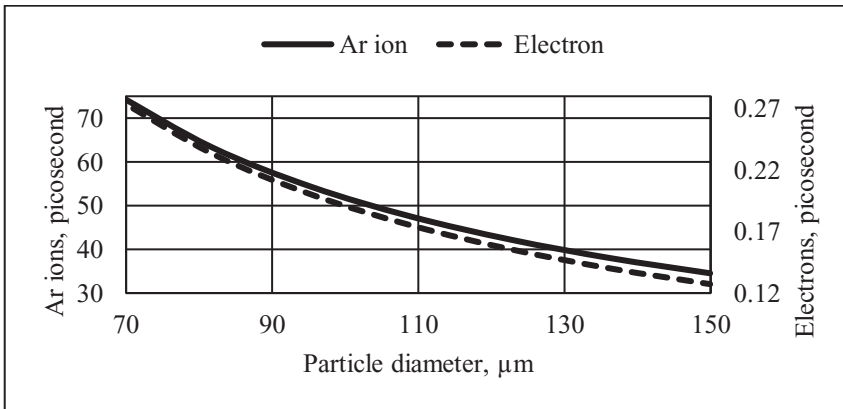


Fig. 6. Characteristic charging time of particles 70-150 μm

The negative charges per particle of the 47, 82 and 140 μm particles are shown in Figure 7 as function of time. The figure shows that the particles reach an equilibrium negative charge below ca. 10^{-9} s of being in the plasma. Thereafter, the charge on the particles remains at the negative equilibrium value for the entire duration in the plasma. The charging process is dynamic, electrons and positive ion will still arrive at the surface of the particle without changing the net charge significantly [13].

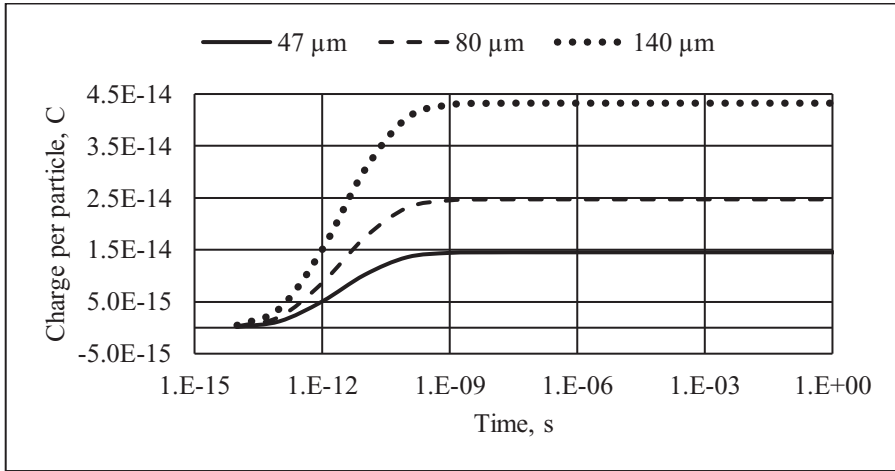


Fig. 7. Charge on Ti6Al4V particles during plasma spheroidisation

The Ti6Al4V particles are introduced as a group into the plasma and the number of particles in a group is controlled by the bulk powder feed rate and the particle size distribution. The group of Ti6Al4V particles will start to repel each other the moment they come in contact with the plasma, as a result of the negative charge acquired by them. The behaviour of the charged particles in the plasma is characterised by the Coulomb coupling parameter. The Coulomb coupling parameter is defined as the ratio of the inter-particle Coulomb potential energy to the thermal energy of the charged particle [5, 14].

Equation 6 is used to calculate the Coulomb coupling parameter [5]. Particles with a Coulomb coupling parameter greater than 170 will form a Coulomb crystal. A Coulomb crystal is a spatially ordered structure that represent an equilibrium between the negatively charged powder particle and the fields that confine the particles [5]. The Coulomb coupling parameter of the particles introduced into the RF plasma at different temperatures are shown in Figure 8. The Ti6Al4V particles are introduced into the centre of the plasma at an initial density and inter-particle spacing of 1.5×10^{11} particle/m³ and 115 μm.

$$\Gamma = \frac{[Q(t)]^2}{4\pi\epsilon_0 dk T_p} \tag{6}$$

Where: Γ is the coulomb coupling parameter, d is the inter-particle spacing (m/particle^{1/3}) and T_p is the particle temperature (K)

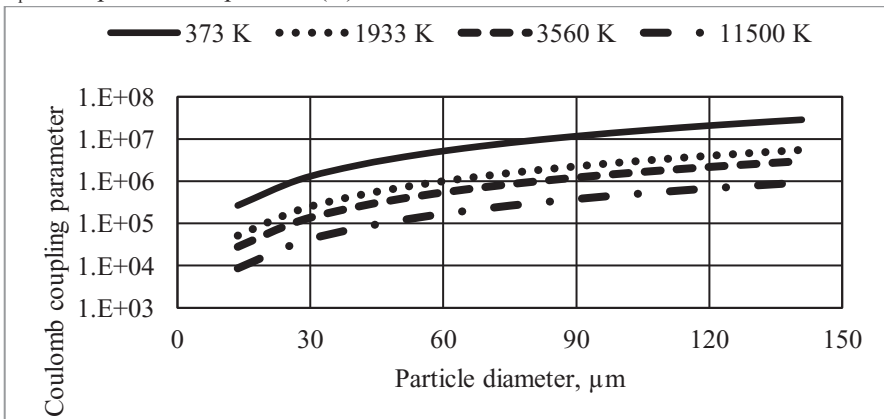


Fig. 8. Coulomb coupling parameter of the particle in an RF plasma

The determined Coulomb coupling parameter was greater than 170 for the Ti6Al4V particles at different temperature. The particles have a high Coulomb coupling parameter when they come in contact with the plasma, provided that particle charging has reached an equilibrium. The Coulomb coupling parameter decreases when the temperature of the particles increases, as shown in Figure 8. However, the Coulomb coupling parameter for the Ti6Al4V particles at 375, 1933, 3560 and 11500 K is still above the minimum value (~ 170), because of the charge acquired from the dense RF plasma ($\sim 3.45 \times 10^{19}$ electrons/m³).

The Ti6Al4V particles will form a Coulomb crystal when they move through the plasma section. Each particle will be surrounded by other particles in all direction, and the distance between the particles will be maintained by the repulsive force that exist amongst the particles. The particles will form a regular polygon shown in Figure 9 [5].

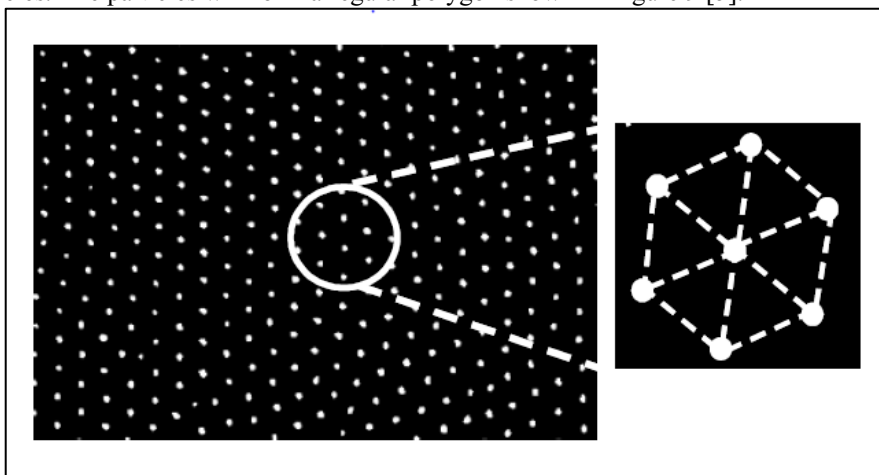


Fig. 9. Typical top view of particles in a plasma [5]

The formation of a Coulomb crystal in the plasma suggests that the particles will exhibit a collective behaviour. A particle will experience a downward force exerted by the particles above it, as a result of the mutual repulsion of the charged particle in the plasma zone. The mutual repulsion of the charged particles prevents particles from colliding with each other even in the molten state. The morphologies of the raw and spheroidised Ti6Al4V are shown in Figure 10. It is evident from the figure that the irregular morphology of the raw Ti6Al4V was transformed to a spherical morphology during the plasma spheroidisation process. The spheroidised particles do not have satellite particles attached to them, as shown on the right image of Figure 10. This is attributed to the negative charge that each particle acquire from the plasma that prevents them from colliding in accordance with Coulomb's law.

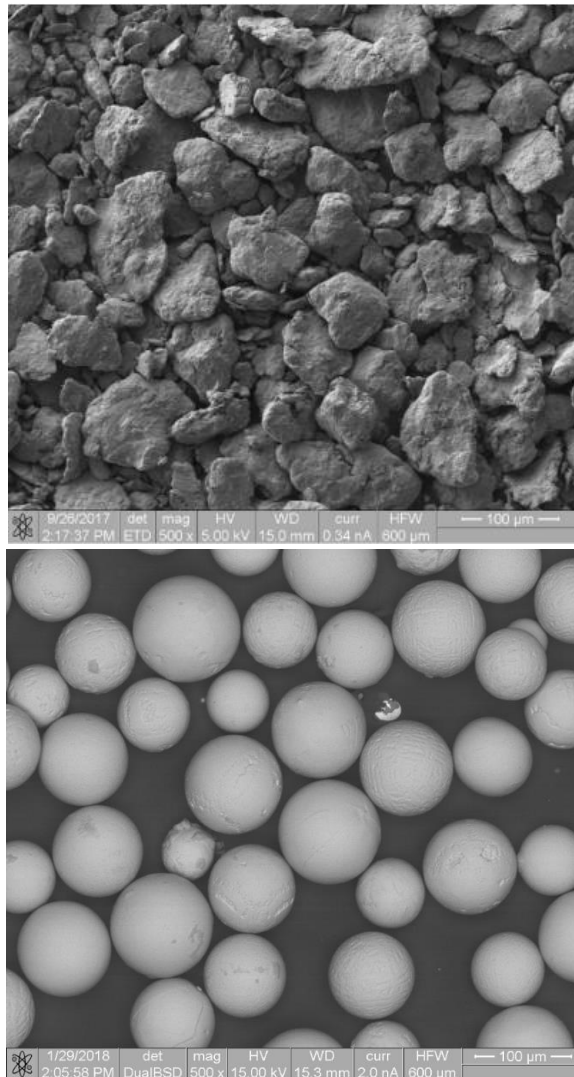


Fig. 10. Top: SEM image of raw Ti6Al4V and Bottom: SEM image of spheroidised Ti6Al4V

4 Conclusions

Particle charging play a significant role during plasma spheroidisation of Ti6Al4V. The study showed that the charge acquired by particle during spheroidisation can result in an ordered arrangement of the particles in the plasma. The ordering of the particles in the form of a Coulomb crystal has an impact when determining the particle flow dynamics in the plasma. Particles charging result in spheroidised particles that do not have satellites attached to their surface.

The Department of Science and Innovation, through the Advanced Material Initiative, and the South African Nuclear Energy Corporation SOC Ltd. (Necsa) is acknowledged for financial support. Mr Patrick Smith is acknowledged for his contribution during the plasma spheroidisation experiments.

Reference

1. H. Bissett and I.J. van der Walt, *J. South. Afr. Inst. Min. Metall.* **117**, pp. 975-980, (2017)
2. Y.L. Li and T. Ishigaki, *J. Am. Ceram. Soc.* **84**, 9, pp. 1929-1936, (2001)
3. "Section 10: Ionization potential of atoms and atomic ions," in *CRC Handbook of Chemistry and Physics*, 83rd Edition, D.R. Lide, London, CRC Press, 2002, pp. 178-180.
4. J. Goree, *Plasma Sources Sci. Technol.* **3**, pp. 400-406, (1994)
5. R.L Merlino, "Dusty plasmas and applications in space and industry", In *Plasma Physics Applied*, C. Grabbe, Transworld Research Network, 2006.
6. M.I. Boulous, P. Fauchais and E. Pfender, "Thermal plasma fundamentals and applications," Volume 1, Springer Science + Business Media, New York, 1994.
7. B.S. Tanenbaum, "Plasma physics", McGraw-Hill, New York, 1967.
8. N.A. Krall and A.W. Trivelpiece, "Principles of plasma physics", San Francisco Press, inc., San Francisco, 1986.
9. J.H. Turner, P.A. Lawless, T. Yamamoto, D.W. Coy, J.D. McKenna, J.C Mycock, A.B. Nunn, G.P. Greiner, W.M. Vatavuk, "Chapter 3: Electrostatic precipitator, Section 6: Particulate matter controls," In *EPA air Pollution Control Cost Manual*, 6th Edition, North Carolina, United State Environmental Protection Agency, 2002, pp. 1-68.
10. M. Pell, J.B. Dunson and T.M. Knowlton, "Section 17: Gas-Solid Operations and Equipment," in *Perry's Chemical Engineers' Handbook*, 8th Edition, New York, D.W. Green and R.H Perry, McGraw-Hill, 2008, pp. 1-64.
11. H.J. White, *Trans. AIEE.* **70**, 1186–1191, (1951)
12. K. Zhang, S. Chen, L. Tan, M. Xu, H. Zhang and D. Zhang, *IOP Conf. Ser. Mater. Sci. Eng.* **677** 032109, (2019)
13. P.M. Bellan, "Fundamentals of Plasma Physics," Cambridge, Cambridge University Press, 2006.
14. J. Kong, K. Qiao, L. Matthews and T. Hyde, *J. Plasma Phys.* **82**, (2016)